

Rods falling near a vertical wall

By **W. B. RUSSEL**,

Department of Chemical Engineering, Princeton University,
Princeton, New Jersey 08540

E. J. HINCH,

Department of Applied Mathematics and Theoretical Physics,
University of Cambridge

L. G. LEAL AND G. TIEFFENBRUCK

Chemical Engineering, California Institute of Technology, Pasadena

(Received 1 November 1976 and in revised form 3 May 1977)

As an inclined rod sediments in an unbounded viscous fluid it will drift horizontally but will not rotate. When it approaches a vertical wall, the rod rotates and so turns away from the wall. Illustrative experiments and a slender-body theory of this phenomenon are presented. In an incidental study the friction coefficients for an isolated rod are found by numerical solution of the slender-body integral equation. These friction coefficients are compared with the asymptotic results of Batchelor (1970) and the numerical results of Youngren & Acrivos (1975), who did not make a slender-body approximation.

1. Introduction

Sedimentation of a sphere through a Newtonian liquid in the absence of inertia is straightforward. In an unbounded fluid the sphere does not rotate and falls in the direction of gravity. The proximity of a vertical wall induces rotation about a horizontal axis parallel to the surface but causes no drift. This well-known behaviour follows from the linearity of the Stokes equations and the symmetry of the geometry.

With rodlike particles a more interesting behaviour can be observed. Taylor (1969) and others have demonstrated that the sedimentation rate of a rod depends on its orientation: a slender cylinder falls approximately twice as fast when it is vertical as it does when it is horizontal. Consequently a rod will drift laterally at intermediate orientations. The absence of rotation, however, again follows from reversibility.

In a tall container the horizontal drift must eventually bring the particle close to a side boundary. Since Batchelor (1970) has demonstrated that the far-field disturbance generated by a rod resembles that of the sphere which encloses it, one might expect interaction with a side to induce rotation. Indeed, this can be observed and is predicted by the far-field analysis of Caswell (1970). Unlike the case of a sphere, however, both the magnitude and the sign of the angular velocity depend on the orientation. According to Caswell's analysis, approach normal to the wall at an inclination of less than 45° to the vertical initially induces a negative angular velocity, i.e. the leading end rotates away from the wall, while at larger angles a positive rotation results. Thus two modes of interaction are suggested (figure 1). A rod approaching at a small angle turns

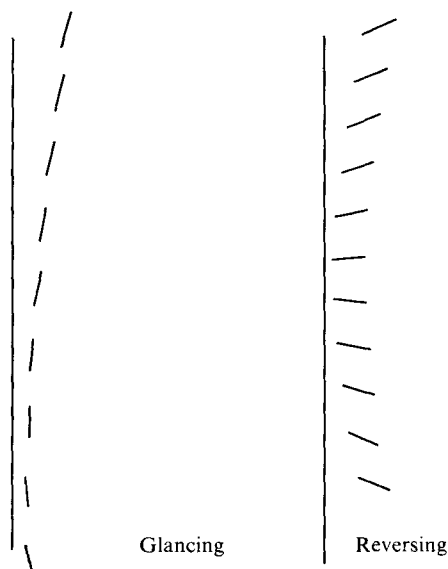


FIGURE 1. Glancing and reversing turns of a sedimenting rod, as predicted by the asymptotic theory of §2, with $\kappa = \frac{1}{60}$. The glancing turn starts from $\theta = 20^\circ$ when $X = 3$ and the reversing turn starts from $\theta = 70^\circ$ when $X = 3$. The rods are shown at time intervals of $4\pi\mu l^2/F_0$.

smoothly through the vertical and drifts away with the same end leading, a 'glancing' turn. At orientations closer to the horizontal the wall primarily retards the near end of the rod, causing it to pivot and then move away with the opposite end leading, a 'reversing' turn. While the far-field analysis indicates the orientation of approach separating the two modes to be 45° , we shall see that terms which have been neglected decrease the critical orientation.

In a tall container there is the possibility of a small rod repeatedly being turned away from the sides before it reaches the bottom. In the case of two vertical sides, symmetry requires the rod to oscillate periodically and not to approach a terminal position or orientation. This effect would lead to a fairly uniform distribution of the rods in the interior of the container, so long as interactions between the rods can be neglected.

The following sections contain an analysis of the interaction between a slender circular cylinder and a single plane wall. We first formulate the problem in terms of slender-body theory and present an asymptotic solution for the instantaneous motion. Then an independent, and more accurate, numerical solution of the integral equations is discussed and the trajectories calculated by the two different approaches are compared. As an aside, numerical results for the friction coefficients of a slender particle in an infinite fluid are compared with the third-order asymptotic solutions of Batchelor (1970) and the non-slender-body results of Youngren & Acrivos (1975). Finally we describe some simple experiments which verify the main theoretical predictions.

2. Theory

Slender-body analysis

Within the past decade slender-body theory, originally proposed for potential flows, has been extensively developed to describe the translation and rotation of rodlike

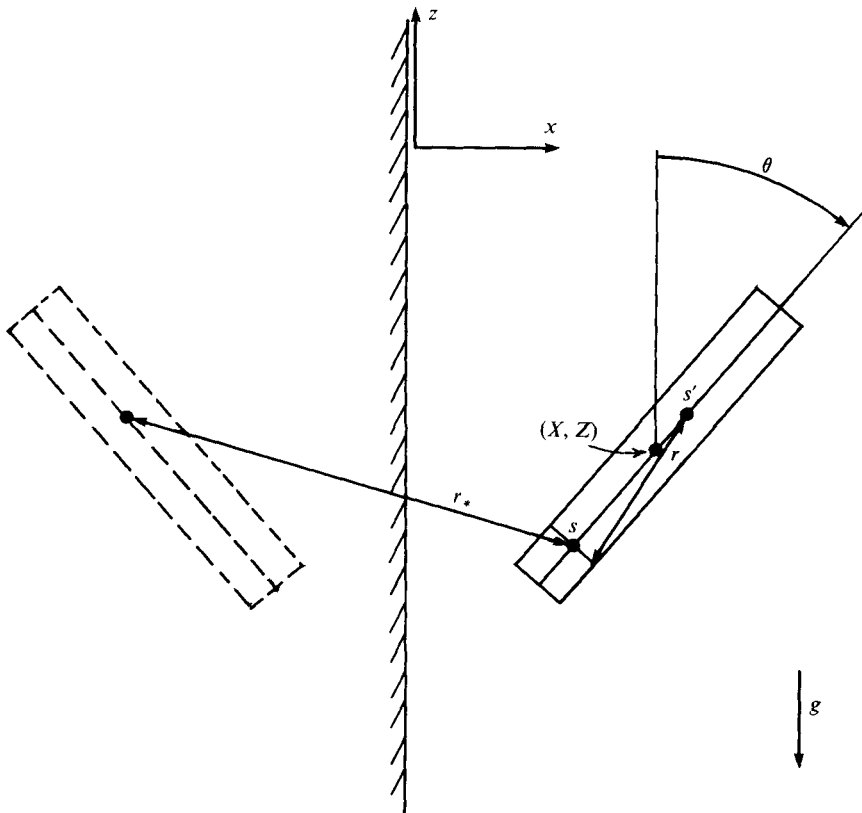


FIGURE 2. The co-ordinate system.

particles at low (zero) Reynolds number. The basic theory has been extended to include the effects of (i) blunt ends (Tuck 1964), (ii) centre-line curvature (Cox 1970), (iii) non-Newtonian suspending fluids (Leal 1975) and (iv) interactions with walls (Blake 1971). Here we use the last development to analyse the motion of a straight slender circular cylinder of radius R_0 and length $2l$ which is sedimenting through a viscous fluid in the vicinity of a plane wall. We assume that the plane of motion of the particle is perpendicular to the wall. Furthermore, end effects are ignored and attention is restricted to situations in which the cylinder is separated from the wall by a distance much greater than R_0 . These simplifications retain most of the interesting physics governing the particle trajectory while making the analysis tractable.

The essence of slender-body theory lies in an approximate representation of the body's effect on the fluid by a distribution of singularities (i.e. point forces, force doublets and source doublets) along its axis. The nature and strength of these singularities are adjusted so that the disturbance flow cancels the applied flow at the particle surface, i.e. there is no slip. If a plane wall is present, an additional set of singularities must be distributed along the axis of the body's image in order to achieve no slip on the wall. The image system for a point force near a plane wall was obtained by Blake (1971). He found it to be a point force of equal magnitude but opposite sign plus a force doublet and a source doublet. These results suffice for our problem.

The co-ordinate system used is illustrated in figure 2, which also serves to define

certain other variables that appear in the theory. The midpoint of the particle is denoted by (X, Z) and its angle of inclination to the vertical by θ . The variables s and s' both specify the position of points on the particle axis relative to its midpoint. The distance between s' and a point on the particle surface at s is denoted by r , while the distance between s and the *image* of s' is denoted by r_* . For convenience, we scale all position and distance variables with respect to l . With these conventions, the two significant disturbance velocities at the cylinder surface are

$$u_x(s) = \frac{1}{8\pi\mu} \int_{-1}^1 \left\{ F_x(s') \left[\frac{1}{r} + \frac{(s-s')^2 \sin^2 \theta + \frac{1}{2}\kappa^2 \cos^2 \theta}{r^3} - \frac{1}{r_*} - \frac{r_*^2(x^2+x'^2) + 6xx'(x+x')^2}{r_*^5} \right] \right. \\ \left. + F_z(s') \cos \theta \left[\sin \theta \frac{(s-s')^2 - \frac{1}{2}\kappa^2}{r^3} - (s-s') \frac{r_*^2(s+s') \sin \theta - 6xx'(x+x')}{r_*^5} \right] \right\} ds', \quad (1a)$$

$$u_z(s) = \frac{1}{8\pi\mu} \int_{-1}^1 \left\{ F_x(s') \cos \theta \left[\sin \theta \frac{(s-s')^2 - \frac{1}{2}\kappa^2}{r^3} + (s-s') \frac{r_*^2(x-x') - 6xx'(x+x')}{r_*^5} \right] \right. \\ \left. + F_z(s') \left[\frac{1}{r} + \frac{(s-s')^2 \cos^2 \theta + \frac{1}{2}\kappa^2 \sin^2 \theta}{r^3} - \frac{1}{r_*} - \frac{(s-s')^2(r_*^2 - 6xx') \cos^2 \theta + 2r_*^2 xx'}{r_*^5} \right] \right\} ds', \quad (1b)$$

where $\kappa = R_0/l$ is the aspect ratio and

$$x = X + s \sin \theta, \quad x' = X + s' \sin \theta,$$

$$r^2 = (s-s')^2 + \kappa^2, \quad r_*^2 = (s-s')^2 + 4X^2 + 4 \sin \theta (sX + s'x).$$

The fluid motion normal to the plane of figure 2 is $O(\kappa)$ and therefore negligible. The appropriate image singularities have been included in (1), so that the boundary condition on the wall is automatically satisfied.

The integral equations (1) are solved by choosing the force distributions $F_x(s)$ and $F_z(s)$ in such a way that the disturbance velocities are of the form of a rigid-body motion:

$$u_x(s) = U_x + \Omega l s \cos \theta, \quad u_z(s) = U_z - \Omega l s \sin \theta. \quad (2)$$

The translational velocity of the rod (U_x, U_z) and its angular velocity Ω are determined by the conditions of constant force and zero couple on the particle:

$$\left. \begin{aligned} \int_{-1}^1 F_x(s) ds = 0, \quad \int_{-1}^1 F_z(s) ds = -F_0 l \\ \int_{-1}^1 [F_x(s) \cos \theta - F_z(s) \sin \theta] s ds = 0. \end{aligned} \right\} \quad (3)$$

and

In the following section, numerical solutions will be presented for the integral equations (1) subject to the side conditions (2) and (3); here we develop an asymptotic solution for the limit $\epsilon = 1/\ln(2/\kappa) \ll 1$.

The asymptotic analysis capitalizes on the quasi-local nature of the slender-body theory; i.e. the fact that the induced velocity at the cylinder's surface primarily depends on the force density at the nearest axial point, as long as the force density varies on a length scale of 1 and not κ . From (1) we have (Batchelor 1970)

$$\left. \begin{aligned} u_x(s) &= (4\pi\mu\epsilon)^{-1} [(1 + \sin^2 \theta) F_x(s) + \sin \theta \cos \theta F_z(s)] + \epsilon v_x, \\ u_z(s) &= (4\pi\mu\epsilon)^{-1} [\sin \theta \cos \theta F_x(s) + (1 + \cos^2 \theta) F_z(s)] + \epsilon v_z, \end{aligned} \right\} \quad (4)$$

where the correction terms v_x and v_z vary with s and are not local. Even when the rod is very near to the wall, i.e. $\theta \sim 0$, $X \ll 1$ and $X/\kappa \gg 1$, de Mestre & Russel (1975) showed that the local nature is preserved with $\epsilon = 1/\ln(2/\kappa)$ in (4) being replaced by $1/\ln(2X/\kappa)$, but for simplicity we suppress this extension by assuming that κ is very much smaller than X . In order to make the disturbance velocities in (4) vary linearly with s as required by (2), we must clearly choose, at lowest order, force distributions which vary linearly with s . The only such force distribution consistent with (3) is

$$F_x = O(\epsilon F_0/l), \quad F_z = -\frac{1}{2}F_0/l, \quad (5)$$

which results in

$$U_x \sim -\frac{\sin\theta \cos\theta}{8\pi\mu\epsilon}F_0, \quad U_z \sim \frac{1 + \sin^2\theta}{8\pi\mu\epsilon}F_0, \quad \Omega = O\left(\frac{F_0}{\mu l^2}\right). \quad (6)$$

Substituting the first approximation to the force distribution (5) into the integral equation (1) yields the correction terms v_x and v_z in (4). The force distributions are then adjusted locally to cancel these corrections. The constraints (3), however, do not permit these adjustments to the force distributions to contain a part which varies linearly with s . The parts of v_x and v_z which vary linearly with s are balanced by adjustments to the translational and rotational velocities U_x , U_z and Ω . Thus we find

$$U_x = -\frac{\sin\theta \cos\theta}{8\pi\mu\epsilon}F_0 + \frac{\epsilon}{2} \int_{-1}^1 v_x(s) ds, \quad (7a)$$

$$U_z = -\frac{1 + \sin^2\theta}{8\pi\mu\epsilon}F_0 + \frac{\epsilon}{2} \int_{-1}^1 v_z(s) ds \quad (7b)$$

and

$$\Omega = \frac{3\epsilon}{2l} \int_{-1}^1 [v_x \cos\theta - v_z \sin\theta] s ds. \quad (7c)$$

After much algebra, evaluating v_x and v_z in (4) and substituting into (7), we find the analytic expression for the angular velocity:

$$\Omega = \frac{3F_0}{32\pi\mu l^2} \left\{ 2XI_0 S^2 + I_1 S(1 + 4S^2) + 2X(2 + 3S^2 - 4S^4) \frac{(X^2 + C^2)^{\frac{1}{2}} - X}{C^2} - 2S^2(1 + 4S^2) \right. \\ \left. - \frac{2X}{(X^2 + C^2)^{\frac{1}{2}}} + L_1 S[X^2(1 + 4S^2) - S^2(3 - 4S^2)] - L_2 XS^2(1 - 4S^2) \right\} [1 + O(\epsilon)], \quad (8)$$

where

$$S = \sin\theta, \quad C = \cos\theta, \quad I_n = \int_{-1}^1 s^n \ln(R_+/R_-) ds, \quad L_1 = \ln \frac{1 + S^2}{A_+ - A_-}, \quad L_2 = \frac{A_+}{A_-},$$

$$R_{\pm} = \{s^2 + 2[2XSF(1 - 2S^2)]s + 1 + 4X^2 \pm 4XS\}^{\frac{1}{2}} \pm 1 + 2XS - s(1 - 2S^2),$$

$$A_{\pm} = [(X^2 + C^2)^{\frac{1}{2}} + XS \pm C^2]/(XFS).$$

Corresponding equations for the translational velocity components can also be obtained. However, the resultant expressions have not been integrated analytically because of their complexity. Instead, for trajectory calculations, we have used the velocities (6a, b) without wall effects. As illustrated by the numerical computations which follow, the dominant error in these approximations lies in the $O(\epsilon)$ and higher corrections to the resistance coefficient rather than the $O(\epsilon/\ln X)$ wall effect. We note that the shape of the slender body does not enter the asymptotic theory at the level of approximation in (8). Thus, although we have worked with a circular cylinder for

simplicity, (8) is applicable to any slender body. In view of its algebraic complexity, we have checked (8) against the theory of de Mestre & Russel (1975) for $\theta = 0$ and $\frac{1}{2}\pi$ and against numerical evaluations of (6a). Furthermore, we have confirmed that $\Omega \rightarrow 0$ as $X \rightarrow \infty$ as expected.

Numerical solution of the integral equation

Slender bodies can be easily constructed with κ sufficiently small for little error to be expected in the predictions of the integral equations resulting from (1). The asymptotic solution (6a, b) and (8) of the integral equations, however, has a more limited application because particles rarely have $\epsilon = 1/\ln(2/\kappa)$ small. For example, in the experiment described in §3 the particles have $\kappa = \frac{1}{80}$ and $\epsilon = 0.209$. A numerical solution of the integral equations was therefore sought to make reasonable predictions for these particles.

The integral equations from the slender-body theory were discretized by dividing the rod into N segments of equal length. Within each segment the Stokeslet force distribution was assumed to have a constant value, introducing $2N$ unknowns, and the integral was evaluated at the centre of each segment, providing $2N$ equations. Care is needed in integrating the kernel function. While the part of the kernel arising from the images in the wall is adequately treated by the trapezoidal rule using the two end points of the segment, such a treatment of the remaining, non-image part of the kernel would result in large, $O(1/\ln N)$ truncation errors. This part was integrated analytically and the resulting analytic expressions rearranged to avoid the numerical subtraction of nearly equal large numbers. The discrete form of the integral equation was thus $2N$ linear equations for the velocity distribution in terms of the $2N$ values of the Stokeslet distribution. While no elements of the coupling matrix vanish, the diagonal is fairly strong, reflecting the singular nature of the integral equation at small κ . A Gauss-Seidel iterative procedure was therefore adopted to solve for the Stokeslet distribution. The iteration was started from the lowest-order asymptotic result and usually converged to an r.m.s. error of 10^{-4} in less than seven iterations. When time stepping the configuration, the iteration was started with the converged result from the previous time step and often required only a single iteration. To avoid systematic errors, the iterative sweep was started from alternate ends at each time step.

To determine the motion of the rod near the wall, three integral equations were solved for each configuration, corresponding to the three velocity distributions for translation of the rod at unit velocity parallel and perpendicular to the wall and for rotation at unit angular velocity. For each velocity distribution, the net force and couple acting on the rod were evaluated from the Stokeslet distributions and the correct linear combination chosen so that the couple vanished and the net force was unity parallel to the wall. This translation and rotation were finally used in a fourth-order Runge-Kutta time-stepping procedure to calculate the next configuration. A step size for which the rod fell through its own length in two time increments generally produced an accuracy of better than 10^{-3} . Smaller time steps are necessary very near the wall, so automatic interval halving was used.

To assess the accuracy of the numerical solution of the integral equation, several studies were performed without the images in the wall. The motion of a rod in an unbounded fluid has received considerable attention and Batchelor's (1970) third-order asymptotic theory is available for comparison. First the effect of increasing N on

the numerical representation of the Stokeslet distribution was studied for perpendicular translation and $\kappa = \frac{1}{60}$. The general shape of the distribution does not change for $N = 3, 7, 15$ and 31 (at which the centre of the end segment is within one radius of the end). Except for the end segments, where the distribution sharply rose by 60%, the predicted values of the force distribution differed by less than $\frac{1}{2}\%$. Varying the length of the numerical segment or subtracting a special analytic end correction might have improved the representation.

The main side study evaluated the various friction coefficients for a free circular cylinder as predicted by the slender-body integral equation. The net forces \mathcal{F}_1 and \mathcal{F}_2 on a rod translating parallel and perpendicular to itself, respectively, were calculated together with the couple \mathcal{L}_2 on a rod rotating about an axis perpendicular to itself and the stresslet \mathcal{S}_{11} when the rod is placed in a pure axially symmetric straining motion. At fixed κ these friction coefficients varied little with N , and the error scaled on $\ln N/N$, as expected from the poor representation of the end regions. For the rotation, the most sensitive of the three coefficients involved in the wall interactions, the result at $\kappa = \frac{1}{60}$ for $N = 10$ had a 7% error and that for $N = 28$ a $3\frac{1}{2}\%$ error. The results for the friction coefficients extrapolated to $N = \infty$ are shown in figure 3, normalized by the first-order asymptotic prediction.

Also shown in figure 3 are Batchelor's (1970) third-order asymptotic results [his equations (8.11)–(8.14)]. At $\kappa = \frac{1}{60}$ the first-order asymptotic results are poor, with the stresslet out by a factor of two. The third-order theory narrows this gap to 13%.

In the case of \mathcal{F}_1 and \mathcal{L}_2 we have in addition been able to compare our results with those of Youngren & Acrivos (1975). They solved numerically the integral equation for Stokeslet singularities distributed on the surface of the rod including the ends, and thereby made no slender-body approximation. Our slender-body numerical results for \mathcal{F}_1 tend quickly to the full numerical results, with an error of 0.4κ coming from the ends. The agreement for \mathcal{L}_2 is not so good, with a 5% difference between the two results at $\kappa = \frac{1}{240}$. (Note that in their table 4 Youngren & Acrivos give the couples multiplied by a factor of 8.) It is not clear whether the discrepancy is due to the slender-body approximation or whether the numerical results are inaccurate at large aspect ratio.

Results

The equations of motion for a rod moving near a wall have been integrated numerically as outlined in the previous subsection. Figure 1 shows the two possible ways in which the rod can turn. Those rods which start far from the wall at an initial inclination to the vertical greater than 67° turn such that they are horizontal at closest approach, while those starting with an initial inclination less than 27° are vertical at their nearest point. Each of the two turns is symmetric under time reversals, so that after the turn the particles tend to the initial inclination to the horizontal but with the opposite sign. Between 27° and 67° the slender-body theory predicts a collision with the wall, although the analysis breaks down for separations less than a diameter. The neglected end effects then become very large and stop the rod from touching the wall. Simple lubrication considerations presented in the appendix suggest that these effects will immobilize the end, causing the rod to pivot through a horizontal position, although this behaviour is not entirely confirmed by the experiments. A detailed analysis of such collisions is complicated by their sensitivity to the precise shape of the end of the rod, with a possibility that the symmetry of the turn would be lost for imperfect ends.

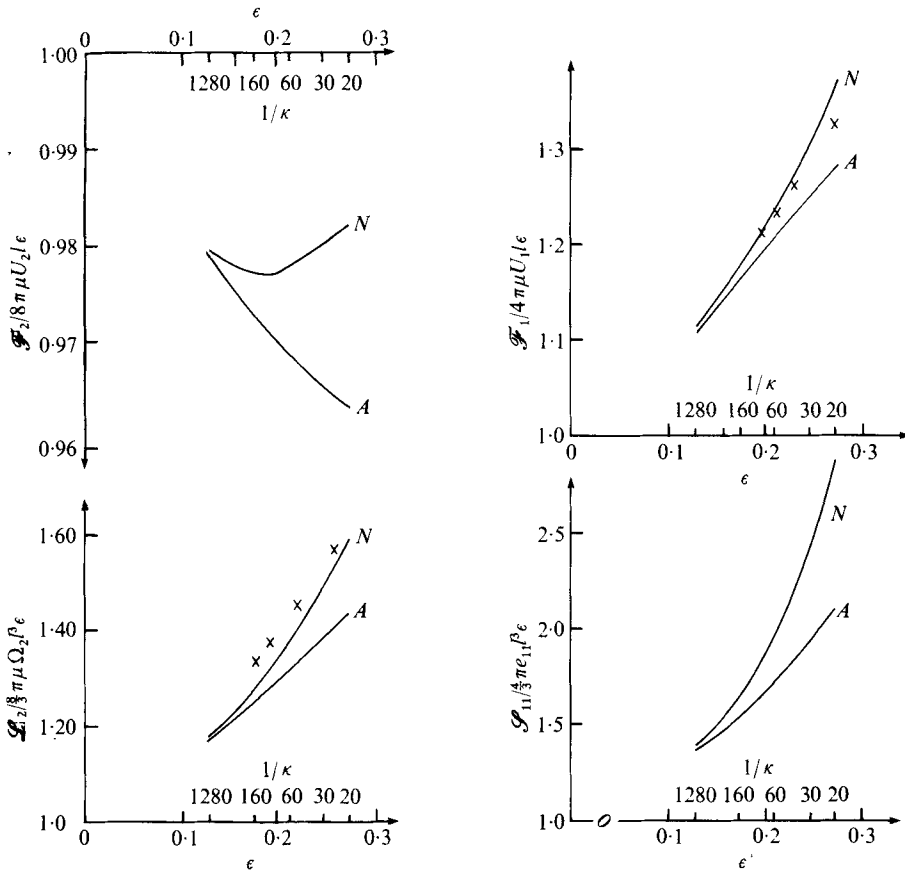


FIGURE 3. The friction coefficients for slender circular cylinders for perpendicular (\mathcal{F}_2) and parallel (\mathcal{F}_1) translation, for rotation about an axis perpendicular to the cylinder (\mathcal{S}_2) and for pure straining motion in the direction of the cylinder (\mathcal{S}_{11}). Our numerical results (N) are compared with Batchelor's third-order asymptotic results (A) and the full numerical results of Youngren & Acrivos (crosses).

In figure 1 the vertical length scale is seen to be large: the rod falls much faster than it moves sideways or rotates. This is particularly evident for the near-vertical glancing turns. An alternative presentation of the results is given in figure 4, where the trajectory is plotted as the inclination from the vertical θ vs. the distance X from the wall to the centre of the rod. Markers at equal time separations ($8\pi\mu l^2/F_0$) are placed along the trajectories. The shaded region denotes the forbidden configurations in which some part of the rod lies within the wall. The trajectories terminating in this region indicate collisions with the wall at finite orientations, even with very fine numerical resolution. Most trajectories show little rotation one particle length from the wall. Rods approaching at 45° , for which the angular velocity vanishes in the far-field analysis of Caswell (1970), rotate through less than 1° before approaching within one quarter of their length from the wall and rotate through only 5° before colliding with the wall. The exceptions are particles which turn at a large distance from the wall. These start near the horizontal or vertical and turn slowly, therefore falling through a large vertical distance before completing the turn.

The full curves in figure 4 are based on the numerical solution of the integral equa-

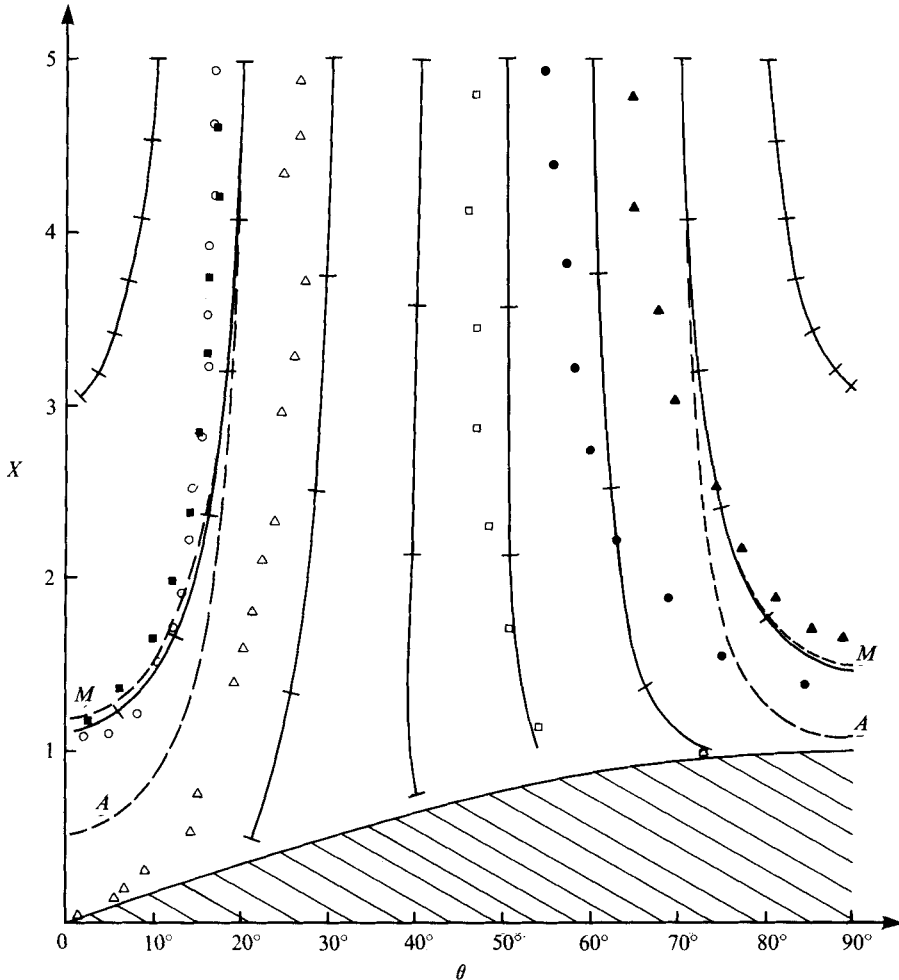


FIGURE 4. The variation of the distance from the wall and the orientation of the rods as they turn. Numerical solution of the integral equation yields the solid curves, which are marked at time intervals of $8\pi\mu l^2/E_0$. The dashed curves labelled *A* are trajectories for 20° and 70° obtained from (6*a*, *b*) and (8). The dashed curves labelled *M* use the modified friction coefficients of figure 3. Experimental data points: \blacktriangle , $\theta_\infty = 65^\circ$; \bullet , $\theta_\infty = 54^\circ$; \square , $\theta_\infty = 47^\circ$; \triangle , $\theta_\infty = 27^\circ$; \circ , $\theta_\infty = 17^\circ$ (run 1); \blacksquare , $\theta_\infty = 17^\circ$ (run 2).

tions. The results from the first-order asymptotic solution of the integral equations are also plotted as dashed curves labelled *A* for the 20° and 70° trajectories. This asymptotic theory underestimates the drag on the rods, allowing them to come much closer to the wall; indeed, the band of initial angles leading to collisions widens to 23° – 69° . Because most of the error in the asymptotic theory comes from the poor friction coefficients for translation, a modified theory was developed in which the numerically evaluated friction coefficients replace the asymptotic ones but the angular velocity remains that of the first-order asymptotic theory. The resulting trajectories for this modified theory, plotted as dashed curves labelled *M*, lie very near the full numerical curves and demand somewhat less computer time. The success of the modified theory indicates that the wall has little effect on the translational velocity of the rods.

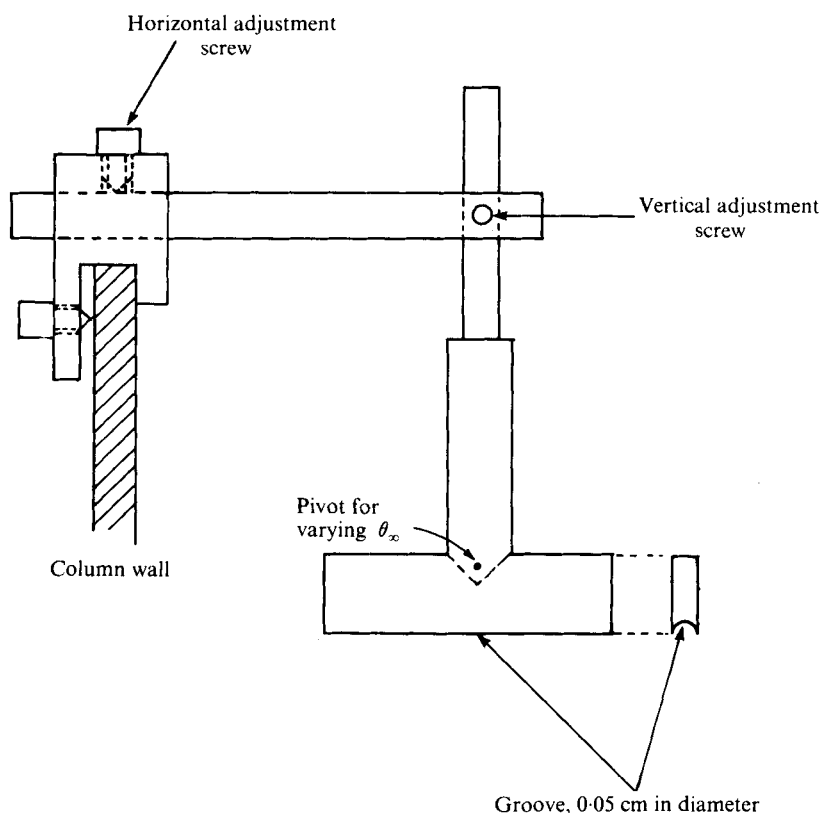


FIGURE 5. The particle release mechanism. Not drawn to scale.

3. Experiment

Apparatus and procedure

The experiments were conducted in a Plexiglas tank with a 2 ft by 2 ft cross-section and a height of 5 ft. The tank was placed on a stand which was adjusted so that the walls were vertical.

The particles were made from aluminium screen wires. These wires were placed between two smooth flat stainless-steel plates and then rolled to a nominal diameter of 0.0254 cm. The aspect ratio $1/\kappa = l/R_0$ of the particles ranged from 59 to 69. A qualitative check with a microscope showed the particles to be straight and of constant radius. The particles were in addition shiny, which made them well suited for photographic study, and light, with a measured density of 2.36 g/cm³.

The liquid used was a white mineral oil supplied by Standard Oil Co. of California. This liquid is colourless and clear, ideally suited for a photographic study. At 22.2 °C, the density of the liquid is 0.88 g/cm³ and its viscosity is 170 cP.

In order that the experiment can be compared with the theory it is important to release the particle in a way which does not cause it to turn out of the plane perpendicular to the wall, or cause a significant disturbance in the surrounding fluid. The release mechanism which we used is shown in figure 5. Its significant feature is the thin metal plate with a groove 0.05 cm in diameter in the bottom edge. Just prior to starting the experiment, the groove is wetted with the liquid being used. The slender

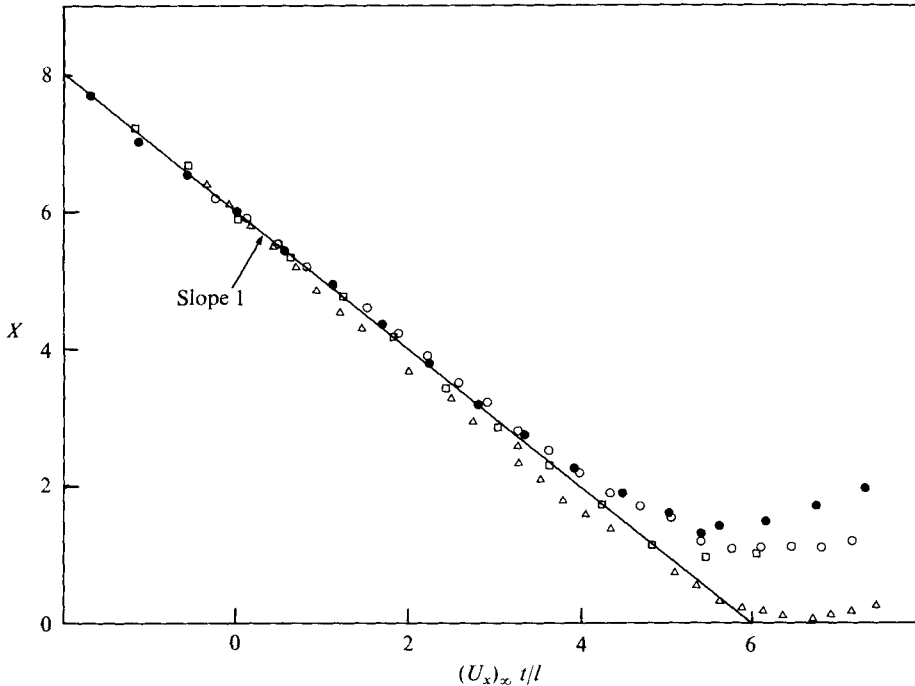


FIGURE 6. Distance between the particle centre and the wall as a function of time. \bullet , $\theta_\infty = 54^\circ$; \square , $\theta_\infty = 47^\circ$; \triangle , $\theta_\infty = 27^\circ$; \circ , $\theta_\infty = 17^\circ$.

body is then carefully placed in the groove. When the plate is submerged in the liquid, the slender body slowly slides out of the groove. The plate can be adjusted such that the particle is released in the proper plane. We found that this system successfully launched about 80% of the particles.

The motion of the particles was recorded on 16 mm cine film with a Bolex camera. The camera was mounted on a counterweighted platform which could be moved up or down at a variable, but controlled speed. The particle was thus tracked during its entire fall, and a continuous film obtained of its trajectory. Quantitative measurements were made from the film using a microfilm reader. Vertical position was measured from image lines on the back of the tank. Horizontal position was determined using a photograph of a ruler taken prior to the experiments. A typical run lasted 5 min, during which thirty frames would be taken at constant intervals.

Results

The purpose of the experiments was to verify, at least qualitatively, the theory described in §2. Thus measurements were made of the position of the particle centre and the particle orientation as functions of time for various initial inclinations ranging from 17° to 65° . We present data here for the five representative cases $\theta_\infty = 17^\circ$ (two sets), 27° , 47° , 54° and 65° , which include one 'glancing' turn (17°), two 'reversing' turns (54° and 65°), one 'colliding' turn (47°), and one turn just on the border between 'glancing' and 'colliding' (27°). Plots showing horizontal and vertical position as a function of time for initial inclinations of 17° , 27° , 47° and 54° are given in figures 6

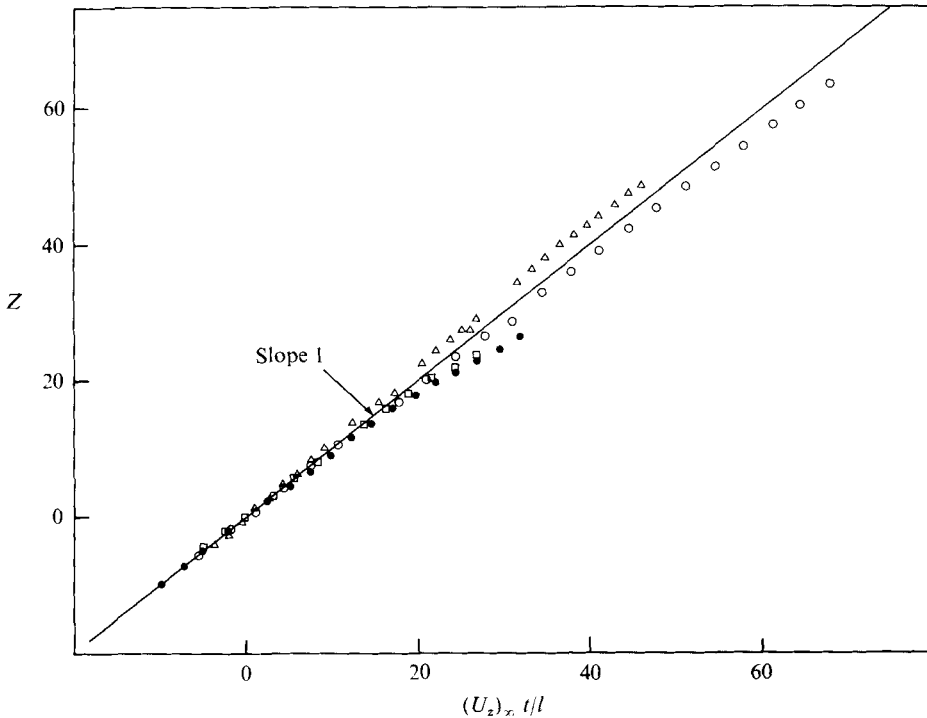


FIGURE 7. Vertical displacement of the particle centre as a function of time. ●, $\theta_\infty = 54^\circ$; □, $\theta_\infty = 47^\circ$; △, $\theta_\infty = 27^\circ$; ○, $\theta_\infty = 17^\circ$.

and 7. The measured angle of inclination as a function of horizontal position for all five initial angles has been superimposed on figure 4, where it may be directly compared with the theoretical results. An indication of the degree of reproducibility of the data is provided by the two independent sets of data for $\theta_\infty = 17^\circ$ in figure 4. We shall discuss figures 4, 6 and 7 in detail shortly.

First, it is useful to consider the motion of the particle when it is far from the wall. All of the experiments were started with the separation between the particle and the wall sufficiently large that the sedimentation rate was constant and the particle rotation nil. The existence of such a regime suggests strongly that both inertia and end effects of the top and bottom of the tank have a negligible influence on the particle motion. For, if inertia or end effects were significant, the particle would rotate and translate with a velocity which varies with time. The absence of a measureable inertia effect is important since the Reynolds numbers based on the observed velocities show values as large as 0.1. A further check on the importance of inertia or end effects is provided by a comparison between the measured velocities and theoretical values corresponding to the drag coefficients of figure 3. The horizontal and vertical velocity components are listed in table 1. The two sets of values are in good agreement, thus confirming the lack of significant inertia or end effects. A final demonstration, which also illustrates a degree of self-consistency in the data, is the fact that the vertical and horizontal positions, plotted *vs.* time in the manner of figures 6 and 7, collapse onto universal curves when the particles are far from the wall.

Turning to the regime of wall interactions, it is clear from figure 4 that the observa-

θ_∞	Experimental		Theoretical	
	U_z	U_x	U_z	U_x
56	0.206	0.0495	0.209	0.048
47	0.210	0.051	0.221	0.050
27	0.265	0.044	0.254	0.041
17	0.255	0.0275	0.265	0.028

TABLE 1. Particle velocities (cm/s).

tions and predictions are at least in qualitative accord. In particular, the ‘glancing’ and ‘reversing’ modes of interaction are both evident, the former for $\theta_\infty = 17^\circ$ and the latter for $\theta_\infty = 54^\circ$ and 65° . In addition, at intermediate angles, e.g. $\theta_\infty = 47^\circ$, the particle appears, with the resolution available, to hit the boundary and then complete its rotation.† Even from a quantitative point of view, the two cases $\theta_\infty = 17^\circ$ and $\theta_\infty = 27^\circ$ are in excellent agreement with theory, certainly well within expectations given the approximations of the theory and uncertainties in the experimental data. The case $\theta_\infty = 27^\circ$ appears to be close to the maximum angle for a ‘glancing’ turn, as the particle comes extremely close to touching the wall.

The three cases of larger initial inclination, $\theta_\infty = 47^\circ$, 54° and 65° , in which the particle undergoes a ‘reversing’ turn, are in poorer agreement with the theory. In particular, the influence of the wall is felt at a much greater distance than that predicted. This is especially evident for $\theta_\infty = 54^\circ$ and 65° , where the particle inclination is already changing when the centre is some 5 half-lengths from the wall. The horizontal velocity is less influenced, but it too begins to be affected by the wall at nearly 3 half-lengths separation distance. We may note that the end of the particle comes very close to touching the wall for $\theta_\infty = 47^\circ$, as predicted by the slender-body theory, but apparently it does not make contact. The strongest evidence for no contact is that the particle continues to slide vertically down the wall, rather than pivoting about a fixed end.

Several other features of the observed particle motions are worth noting. First, the particle trajectories are reversible. We have only shown data corresponding to the approach to the boundary. However, complete symmetry was observed between the approach and retreat. This is true even for $\theta_\infty = 47^\circ$, where the particle end is very close to the wall, thus providing further evidence that the particle and wall do not touch. Second, the angle of inclination appears more sensitive to the influence of the wall than any of the other variables. In particular, the plots of figures 6 and 7 show close agreement with predicted translational velocities in an infinite fluid, right down to one half-length separation between the wall and particle. Indeed, except for separations of one half-length or smaller, deviations from the infinite-fluid result are well within normal experimental error, and probably of little significance.

Clearly, most features of the motion of rod-like particles near a plane wall are correctly predicted by the slender-body analysis of §2. Some points of disagreement, for example the lack of contact between particle and wall for $\theta_\infty = 47^\circ$, may result from end corrections neglected in the analysis. Other points of disagreement, however, are

† We shall discuss this last point in more detail later.

not so easily explained and thus require further study. Most important are the deviations between theory and experiment which are found at large distances when the initial inclination is large (i.e. $\theta_\infty = 54^\circ$ and 65°). At present, we see no obvious explanation for these differences either in the theory or in experiments.

L. G. Leal and G. Tieffenbruck wish to thank the National Science Foundation for its support of their participation in this work, through grant ENG 74-17590.

Appendix. A lubrication theory for a 'colliding' turn

The way in which lubrication forces acting on the end of the rod manage to stop it colliding with the wall makes an interesting study for the method of matched asymptotic expansions. Here we summarize the basic results. Time is non-dimensionalized by $4\pi\mu l/F_0$ and lengths remains non-dimensionalized by the half-length of the rod. For simplicity we assume that the rod has a spherical end of radius κR with R of order unity. Except for lubrication forces acting on the end, no interaction with the wall is included as appropriate at the lowest order of slender-body theory.

The standard expressions for the lubrication forces become applicable when the separation d between the rod and the wall is somewhat smaller than κ , i.e. the thickness of the rod. These lubrication forces do not affect the motion, however, until $d = O(\kappa^2 \ln \kappa)$, because the friction coefficient for the whole rod is $1/\kappa \ln \kappa$ larger than that for the small end. Initially only the normal lubrication force acts, and it dramatically slows down the horizontal motion towards the wall. The normal force also causes a negative angular velocity.

The tangential lubrication force becomes important after a short time $O(\kappa \ln \kappa)$, when

$$d = O(\kappa^2 \exp(5 \cos^2 \theta/R \kappa \ln \kappa)).$$

This occurs in spite of the fact that the friction coefficient associated with the tangential lubrication force is $O((d/\kappa) \ln(d/\kappa))$ smaller than that associated with the normal force, because the normal velocity drops more dramatically than the tangential velocity. The action of the tangential lubrication force is to decrease the tangential velocity of the end of the rod, and to make the rod rotate with a positive angular velocity.

There then follows a long phase in which the rod rotates virtually pivoting on a fixed end. The pivoting turn lasts for a period of time

$$\frac{3}{4} \frac{1}{\ln \kappa} \ln \left(\tan \frac{\theta_\infty}{2} \right).$$

During the turn the end of the rod slips vertically a distance $O(\kappa)$ while the minimum separation is predicted to be

$$d = \kappa^2 R^2 \exp \left(\frac{3}{8} \sin \theta_\infty / \kappa^2 \ln \kappa R^2 \right).$$

This minimum separation is extremely small; indeed, so small that physical contact must be expected in practice, e.g. in the experiments of §3 a separation smaller than 10^{-100} m is predicted. Physical contact, or any other breakdown of the lubrication theory, would of course destroy the symmetry of the turn. The reason for the smallness of the minimum separation is not difficult to see: the normal lubrication force

$$\frac{3}{4} \kappa^2 R^2 \dot{d}/d$$

remains $O(1)$ during the turn, which lasts for $1/\ln \kappa$, thus $\ln(d/d_0) = O(1/\kappa^2 \ln \kappa)$.

REFERENCES

- BATCHELOR, G. K. 1970 *J. Fluid Mech.* **44**, 419.
BLAKE, J. R. 1971 *Proc. Camb. Phil. Soc.* **70**, 303.
CASWELL, B. 1970 *Chem. Engng Sci.* **27**, 373.
COX, R. G. 1970 *J. Fluid Mech.* **44**, 791.
LEAL, L. G. 1975 *J. Fluid Mech.* **69**, 305.
MESTRE, N. J. DE & RUSSEL, W. B. 1975 *J. Engng Math.* **9**, 81.
TAYLOR, G. I. 1969 In *Problems of Hydrodynamics and Continuum Mechanics*, p. 718. SIAM Publ.
TUCK, E. O. 1964 *J. Fluid Mech.* **18**, 619.
YOUNGREN, G. K. & ACRIVOS, A. 1975 *J. Fluid Mech.* **69**, 377.